Magnetic Barrier in Front of Exoplanets Interacting with Stellar Wind

Nikolai V. Erkaev and **Kseniya D. Gorbunova**

Abstract The interaction between the magnetized stellar wind plasma and the hydrodynamic flow from the upper atmosphere of a non-magnetic exoplanet is studied. The recently discovered warm Neptune TOI-421c is considered as an example of such an interaction. The obstacle boundary is determined by the condition of pressure balance between the stellar wind and the expanded atmosphere. Extreme ultraviolet stellar radiation drives a hydrodynamic supersonic outflow of hydrogen atoms. Neutral atmospheric atoms penetrate the region of the stellar wind, where they are ionized and mixed with the stellar wind plasma. The 3D MHD model was applied to calculate the detached bow shock and the magnetosheath region between the shock and the streamlined surface-ionopause. We have obtained a thick magnetic barrier, characterized by a strong increase in the magnetic field and total pressure, a decrease in the velocity, pressure and temperature of the plasma. An enhanced magnetic field shifts the ionopause towards the planet.

Keywords Exoplanets · Stellar wind · Planetary wind · Magnetic barrier

1 Introduction

Planets located outside the Solar system are called exoplanets. Observing such planets was a very difficult task because they have low luminosities compared to their host stars. The first exoplanets were discovered about 30 years ago. Recently, thanks to a new precise observation technique, many exoplanets have been discovered. The escape of atmospheric particles under the influence of high-energy stellar radiation is a key phenomenon that determines the structure and evolution of the planetary atmospheres. The properties of planetary atmospheres are closely related to the integral radiation flux received by planets during their existence and also to the evolution track of their host stars. In the early stages of evolution, a significant extreme ultraviolet

© The Author(s), under exclusive license to Springer Nature Switzerland AG 2023
A. Kosterov et al. (eds.), *Problems of Geocosmos—2022*, Springer Proceedings in Earth and Environmental Sciences, https://doi.org/10.1007/978-3-031-40728-4_18

radiation (EUV) from the host star causes an intense loss of planetary atmospheres. Another aspect is the interaction of outgoing atmospheric particles with the stellar wind consisting of protons and electrons in the presence of the interplanetary magnetic field (IMF). More than two decades ago, a number of publications have shown that the IMF plays an extremely important role in the interaction between the solar wind and the planets of the solar system. In particular, the Pioneer Venus Orbiter observed the so-called magnetic barrier in front of the Venusian ionosphere [1]. Since planet Venus has no own magnetic field, the observed enhanced magnetic field in the magnetic barrier was considered as an induced magnetic field in the region of solar wind flow around the ionosphere [2]. A similar induced magnetic field has also been observed in the Martian environment [3]. But non-magnetic planets are not the only objects where a magnetic barrier can form. This phenomenon also occurs when the solar wind flows around magnetic planets such as Earth, Jupiter, and Saturn [4]. Thus, the magnetic barrier is a fairly general phenomenon that occurs when a magnetized plasma (solar/stellar wind) flows around impenetrable obstacles (the magnetosphere or ionosphere) [5]. And the recently discovered exoplanet TOI-421c, flown around by a stellar wind, has all conditions for the formation of the magnetic barrier which is the aim of our present study.

Mathematical modeling of the escaping planetary atmospheres interacting with the stellar wind in combination with observations can provide important additional information concerning the physical conditions on specific planets.

Using the known characteristics of the exoplanet TOI-421c, we consider two consecutive mathematical models: (1) A hydrodynamic model of a supersonic radial outflow of atmospheric particles (planetary wind) caused by extreme ultraviolet heating of the upper atmosphere; (2) MHD model of a magnetized stellar wind flow around an obstacle formed as a result of its interaction with the planetary wind. The first model gives radial profiles of temperature, pressure, and density of atmospheric particles used to calculate the radius of the obstacle (distance to the stagnation point where the stellar wind stops). The obstacle surface called as ionopause separates the internal atmospheric ions from the external stellar wind protons. Also, the density, velocity, and temperature of atmospheric atoms penetrating the stellar wind region are used in the second model to determine the sources of mass, momentum, and energy due to photo-ionization and charge exchange processes.

2 Model Equations and Statement of Problem

Geometrical situation of interaction between the incoming EUV radiation and planetary atmosphere is illustrated in Fig. 1. Here the X axis points to the host star, the planetary wind is marked by the light blue arrows pointed to the radial directions, and the EUV flux is shown by the dark blue arrows directed opposite to the X axis. The stellar wind is shown by the red arrows at the top of the figure. The interplanetary magnetic field is directed perpendicular to the stellar wind velocity. We split the whole problem into two parts: (a) Formation of the supersonic planetary wind,

Fig. 1 Illustration of the geometrical situation of planetary wind driven by EUV absorption
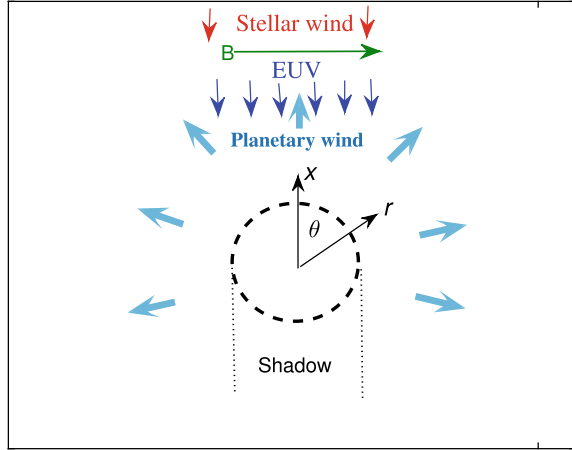
and (b) Interaction between the stellar wind and atmospheric particles. To study the atmospheric escape process, a one-dimensional hydrodynamic model of the upper atmosphere was applied, based on solving the equations of conservation of mass, momentum, and energy [6, 7]

$$\frac{\partial(\rho r^2)}{\partial t} + \frac{\partial(\rho v r^2)}{\partial r} = 0, \tag{1}$$

$$\frac{\partial(\rho v r^2)}{\partial t} + \frac{\partial[(\rho v^2 + p)r^2]}{\partial r} = -\rho r^2 \frac{\partial \Phi}{\partial r} + 2pr, \tag{2}$$

$$\frac{\partial[r^2(0.5\rho v^2 + E_{th})]}{\partial t} + \frac{\partial[r^2 v(0.5\rho v^2 + E_{th} + p)]}{\partial r} =$$
$$-\rho v r^2 \frac{\partial \Phi}{\partial r} + r^2 \frac{\rho_n}{m}\left[Q - \Lambda \exp\left(-\frac{118348}{T}\right)\frac{\rho_i}{m}\right], \tag{3}$$

$$Q = \eta \sigma_i J_\infty \left[0.5 \int_0^{\frac{\pi}{2}+\arccos(\frac{R_p}{r})} \exp(-\tau)\sin(\theta)d\theta \right], \tag{4}$$

$$\tau = \int_r^\infty \frac{\sigma_i}{m} \frac{\rho_n(s)s\,ds}{(s^2 - r^2\sin(\theta)^2)^{1/2}}. \tag{5}$$

Here, coefficient Λ is related to the Layman-alpha cooling radiation ($\Lambda = 7.5 \cdot 10^{-19}$ erg cm^3 s^{-1}); ρ, v, p, T are the mass density, velocity, thermal pressure and temperature; m is the mass of hydrogen atoms; E_{th} is the thermal

energy of hydrogen atoms per unit volume ($E_{th} = 3/2p$); η is the so called heating efficiency, which is estimated from the common approximation that the whole XUV flux is emitted at the energy of 20 eV and thus $\eta = 1 - (13.6\,\text{eV}/20\,\text{eV}) \approx 0.32$ [8]; function Q determines the EUV heating rate; Φ is the gravitational potential; r is the radial distance from the center of planet; θ is the spherical angle counted from the direction of star; σ_i is the ionization cross section, and J_∞ is the extreme ultraviolet radiation intensity (in units "erg cm^{-2} s^{-1}") incoming from the host star far away from the planet; ρ_i and ρ_n are the densities of ions and neutral atoms, respectively.

Using the 2-D heating function averaged over the spherical and azimuthal angles, as given by Eq. (4), is computationally expensive. Therefore, it is convenient to implement a 1-D approximation of the heating function as follows

$$Q = \sigma_i \eta J_\infty \exp(-\tau)/(1 + \epsilon\tau), \quad \tau = \int_r^\infty (\sigma_i/m)\rho_n(s)ds.$$

Here, ϵ is a fitting parameter. The absorption of the EUV radiation leads to heating of the upper atmosphere, as well as to the dissociation and ionization of the atmospheric particles. Densities of the neutral and ionized particles are determined from the following system of equations

$$\frac{\partial \rho_n}{\partial t} + \frac{1}{r^2}\frac{\partial(\rho_n v r^2)}{\partial r} = -\nu\rho_n + \alpha n_e \rho_i. \tag{6}$$

$$\frac{\partial \rho_i}{\partial t} + \frac{1}{r^2}\frac{\partial(\rho_i v r^2)}{\partial r} = \nu\rho_n - \alpha n_e \rho_i. \tag{7}$$

Here, ρ_n and ρ_i are the mass densities of the neuteral and ionized hydrogen atoms, respectively; n_e is the electron density, determined by the quasi-neutrality condition $n_e = \rho_i/m$; ν is the photo-ionization rate and α is the recombination rate

$$\nu = 0.59 \cdot 10^{-7} \cdot J_\infty \frac{\exp(-\tau)}{(1 + \epsilon\tau)}\,\text{s}^{-1}, \quad \alpha = 2.7 \cdot 10^{-13}\left(\frac{10^4}{T}\right)^{0.9}\,\text{cm}^3\,\text{s}^{-1}.$$

Pressure p is defined as the sum of partial pressures of neutral atoms, ions and electrons

$$p = k_B T(\rho_n/m + \rho_i/m + n_e),$$

where k_B is the Boltzmann constant.

2.1 Normalized Equations

For the convenience of calculations, we introduce normalized quantities as follows

$$\tilde{p} = p/(\rho_0 v_0^2),\ \tilde{\rho} = \rho/\rho_0,\ \tilde{v} = v/v_0,\ \tilde{T} = T/T_0,$$
$$\tilde{r} = r/R_p,\ \tilde{t} = tv_0/R_p,\ v_0 = \sqrt{k_B T_0/m}, \xi = \rho_i/\rho,$$

where ρ_0 and T_0 are the mass density and temperature at the planetary boundary, R_p is the planetary radius. The normalizations introduced above make it possible to transform the system of Eqs. (1)–(5), (6), (7) to the following form

$$\frac{\partial(\tilde{\rho}\tilde{r}^2)}{\partial \tilde{t}} + \frac{\partial(\tilde{\rho}\tilde{v}\tilde{r}^2)}{\partial \tilde{r}} = 0, \tag{8}$$

$$\frac{\partial(\tilde{\rho}\tilde{v}\tilde{r}^2)}{\partial \tilde{t}} + \frac{\partial[(\tilde{\rho}\tilde{v}^2 + \tilde{p})\tilde{r}^2]}{\partial \tilde{r}} = -\tilde{\rho}\lambda + 2\tilde{p}\tilde{r}, \tag{9}$$

$$\frac{\partial[\tilde{r}^2(0.5\tilde{\rho}\tilde{v}^2 + 1.5\tilde{p})]}{\partial \tilde{t}} + \frac{\partial[\tilde{r}^2\tilde{v}(0.5\tilde{\rho}\tilde{v}^2 + 2.5\tilde{p})]}{\partial \tilde{r}} = -\tilde{\rho}\tilde{v}\lambda +$$
$$\tilde{r}^2\tilde{\rho}(1 - \xi)\left[\tilde{Q} - \tilde{\rho}\xi\tilde{\Lambda}\exp(-B/\tilde{T})\right], \tag{10}$$

$$\tilde{Q} = 0.5q_0 \int\limits_{0}^{\pi/2+\arccos(\frac{1}{\tilde{r}})} \exp(-\tau)\sin(\theta)d\theta \tag{11}$$

$$\tau = a_0 \int\limits_{r}^{\infty} \tilde{\rho}(s)(1 - \xi)\frac{sds}{(s^2 - r^2\sin(\theta)^2)^{1/2}}, \tag{12}$$

$$\frac{\partial(\tilde{\rho}\xi)}{\partial \tilde{t}} + \frac{1}{r^2}\frac{\partial(\tilde{\rho}\xi\tilde{v}\tilde{r}^2)}{\partial \tilde{r}} = \tilde{v}\tilde{\rho}(1 - \xi)\frac{\tilde{Q}}{q_0} - \tilde{\alpha}\tilde{\rho}^2\xi^2. \tag{13}$$

Here, the normalized pressure is a function of the density, temperature and ion fraction: $\tilde{p} = (1 + \xi)\tilde{\rho}\tilde{T}$, the dimensionless constant parameters in Eqs. (9)–(13) are defined as follows

$$\lambda = G\frac{mM_p}{R_p k_B T_0}, \quad a_0 = \sigma_i \rho_0 R_p/m, \quad q_0 = \sigma_i \eta J_\infty \frac{R_p m^{1/2}}{(k_B T_0)^{3/2}},$$

$$\tilde{\Lambda} = \Lambda\frac{\rho_0 R_p}{m^2 v_0^3}, \quad B = \frac{118348}{T_0}, \quad \tilde{\nu} = 0.59 \cdot 10^{-7} \cdot J_\infty \frac{R_p}{v_0},$$

$$\tilde{\alpha} = 2.7 \cdot 10^{-13}\left(\frac{10^4}{T_0}\right)^{0.9}\frac{\rho_0 R_p}{m v_0}, \tag{14}$$

where G is the gravitational constant, M_p is the planetary mass. As a result of heating, a radial outflow of atmospheric particles can be formed. In this case, the most interesting and important process is that so called "blow-off" aerodynamic

regime, in which the gas velocity monotonically increases to supersonic values with distance from the planet.

3 Numerical Method

System of Eqs. (8)–(13) can be written in the following vector form

$$U_t + \{G(U)\}_r = S(U).$$

Introducing numerical grid ($t_j = j\Delta t$, $r_k = 1 + k\Delta r$, $k = 0, 1, 2, \ldots, N$), we apply the compact MacCormack-type scheme with high accuracy [9, 10]. In particular, we use the 4th order accuracy scheme [11], in which the solution at each time step is calculated in 4 stages as follows

$$U^{j+1} = U^j + \delta_1 h^{(1)} + \delta_2 h^{(2)} + \delta_3 h^{(3)} + \delta_4 h^{(4)}, \tag{15}$$

where $\delta_1 = \frac{1}{6}, \delta_2 = \frac{1}{3}, \delta_3 = \frac{1}{3}, \delta_4 = \frac{1}{6}$, and

$$h^{(1)} = -\Delta t D^F[G(U^j)] + \Delta t S(U^j), \tag{16}$$
$$h^{(2)} = -\Delta t D^B[G(U^j + \alpha_2 h^{(1)})] + \Delta t S(U^j + \alpha_2 h^{(1)}), \tag{17}$$
$$h^{(3)} = -\Delta t D^F[G(U^j + \alpha_3 h^{(2)})] + \Delta t S(U^j + \alpha_3 h^{(2)}), \tag{18}$$
$$h^{(4)} = -\Delta t D^B[G(U^j + \alpha_4 h^{(3)})] + \Delta t S(U^j + \alpha_4 h^{(3)}), \tag{19}$$

Here, $\alpha_2 = 1/2, \alpha_3 = 1/2, \alpha_4 = 1$; $D^F(f)$ and $D^B(f)$ are the forward and backward finite difference approximations of the derivative of a function f with respect to r, which are determined by the following recurrent formulas

$$A D_{k-1}^B + (1-A) D_k^B = \frac{1}{\Delta x}(f_k - f_{k-1}), \tag{20}$$

$$A D_{k+1}^F + (1-A) D_k^F = \frac{1}{\Delta x}(f_{k+1} - f_k), \tag{21}$$

where $A = \frac{1}{2}(1 - \frac{1}{\sqrt{3}})$. The recurrent equations require the boundary conditions, which are determined by the corresponding boundary stencils as follows

$$D_0^F = \left[\left(-\tfrac{25}{12} + \tfrac{17}{12\sqrt{3}}\right) f_0 + \left(4 - \tfrac{25}{6\sqrt{3}}\right) f_1 - \left(3 - \tfrac{3\sqrt{3}}{2}\right) f_2 + \right.$$
$$\left. + \left(\tfrac{4}{3} - \tfrac{13}{6\sqrt{3}}\right) f_3 - \left(\tfrac{1}{4} - \tfrac{5}{12\sqrt{3}}\right) f_4\right] \tfrac{1}{\Delta r},$$
$$D_0^B = \left[-\left(\tfrac{25}{12} + \tfrac{17}{12\sqrt{3}}\right) f_0 + \left(4 + \tfrac{25}{6\sqrt{3}}\right) f_1 - \left(3 + \tfrac{3\sqrt{3}}{2}\right) f_2 + \right.$$
$$\left. + \left(\tfrac{4}{3} + \tfrac{13}{6\sqrt{3}}\right) f_3 - \left(\tfrac{1}{4} + \tfrac{5}{12\sqrt{3}}\right) f_4\right] \tfrac{1}{\Delta r},$$
$$D_N^F = \left[\left(\tfrac{25}{12} + \tfrac{17}{12\sqrt{3}}\right) f_N - \left(4 + \tfrac{25}{6\sqrt{3}}\right) f_{N-1} + \left(3 + \tfrac{3\sqrt{3}}{2}\right) f_{N-2} - \right. \tag{22}$$
$$\left. - \left(\tfrac{4}{3} + \tfrac{13}{6\sqrt{3}}\right) f_{N-3} + \left(\tfrac{1}{4} + \tfrac{5}{12\sqrt{3}}\right) f_{N-4}\right] \tfrac{1}{\Delta r},$$
$$D_N^B = \left[\left(\tfrac{25}{12} - \tfrac{17}{12\sqrt{3}}\right) f_N - \left(4 - \tfrac{25}{6\sqrt{3}}\right) f_{N-1} + \left(3 - \tfrac{3\sqrt{3}}{2}\right) f_{N-2} - \right.$$
$$\left. - \left(\tfrac{4}{3} - \tfrac{13}{6\sqrt{3}}\right) f_{N-3} + \left(\tfrac{1}{4} - \tfrac{5}{12\sqrt{3}}\right) f_{N-4}\right] \tfrac{1}{\Delta r}.$$

With the condition (22) for D_0^B we calculate D_k^B from (20) in the direction of increasing grid number k: $k = 0, 1, 2, \ldots, N$. Then, starting with the condition (22) for D_N^F, we calculate D_k^F from (21) in the opposite direction of decreasing grid number k: $k = N, N-1, N-2 \ldots 0$. After that, we substitute the obtained quantities D^B and D^F into formulas (16)–(19) to determine the intermediate parameters $h^{(1)}, h^{(2)}, h^{(3)}, h^{(4)}$ used in (15) to calculate the solution at the next time step.

Applying this numerical method, we have calculated a non-stationary solution of the equations of hydrodynamics describing a radial loss of the atmospheric particles. This solution evolves in time to unique stationary profiles of the atmospheric density, velocity and temperature, which do not depend on the chosen initial condition. In particular, a hydrostatic isothermal density distribution can be used as a possible initial condition. Near the surface of the planet, we establish boundary conditions for temperature and density. And at the upper boundary for a sufficiently large radius, where the flow is supersonic, we set the so-called "free" conditions, which mean zero derivatives of velocity, density and temperature. These conditions do not affect lower atmosphere due to the supersonic nature of the flow.

4 Outflow of the Atmospheric Particles

As a simulation object, we consider the real exoplanet TOI-421c (warm Neptune), which was first observed by TESS mission in 2020 [12]. This planet is disposed at distance about 244 light years from Earth and has the following physical parameters: $M_p = 16.42\ M_E$, $R_p = 5.09\ R_E$, $T_0 = 673.6$ K, $J_\infty = 1655$ erg cm^{-2} s^{-1}, where M_E and R_E are the mass and radius of Earth, respectively. It is assumed that the atmosphere consists of hydrogen atoms. Results of hydrodynamic calculation of the atmospheric profiles are presented in Figs. 2 and 3. In particular, Fig. 2 shows the heating rate function per 1 particle (solid curve), hydrodynamic (dot-dash) and hydrostatic (dash) density profiles corresponding to exoplanet TOI-421c with the following dimensionless model parameters (14): $\lambda = 36$, $q_0 = 81$, $a_0 = 3.3 \cdot 10^8$. One can see, that the hydrodynamic and hydrostatic density profiles coincide each
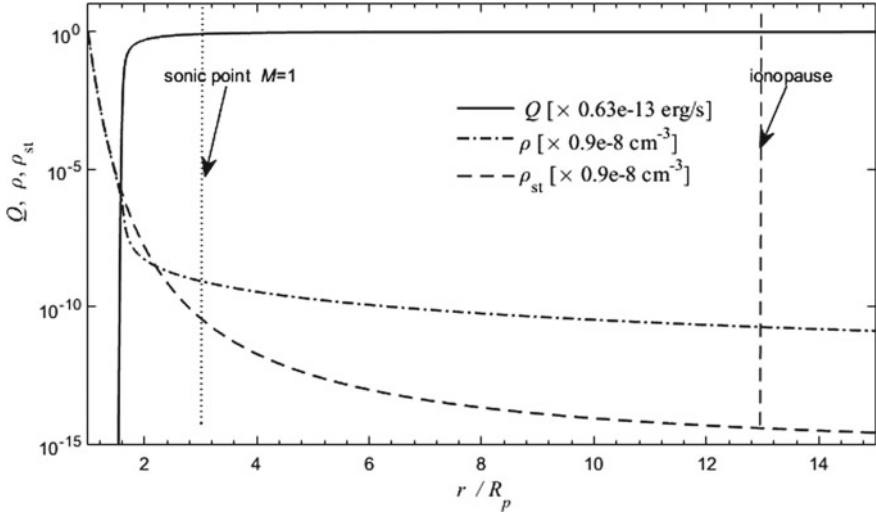
Fig. 2 Hydrodynamic and thermostatic mass densities, and heating source as functions of the radial distance. The dotted and dashed vertical lines indicate critical sonic point and the ionopause position, respectively

other at distances $r \leq 1.5$ (in units of R_p), where the heating function shows a very abrupt decrease.

The left panel of Fig. 3 demonstrates the radial profiles of the temperature and ion fraction (ρ_i / ρ) corresponding to warm Neptune TOI-421c. The temperature increases steeply by a factor of 6 within the region below $r = 4R_p$, where it reaches its maximum of about 6000 K. Above this point, the temperature gradually decreases in the region of supersonic flow due to adiabatic cooling. The right panel of Fig. 3 depicts the radial profiles of velocity and sonic Mach number. The radial velocity gradually increases with radial distance and reaches supersonic values at $r \geq 3R_p$. The velocity maximum is about 20 km/s.

5 MHD Model of Stellar Wind Flow

At some distance from the planet, the supersonic planetary wind forms an obstacle to the oncoming stellar wind that flows around such an obstacle. Stellar wind interaction with the planetary wind was simulated in the model [13] in the framework of pure hydrodynamic approach for the stellar wind, and the interplanetary magnetic field was not taken into account. We apply the MHD model described in [14], which incorporates the arbitrary directed IMF in the stellar wind. We approximate the dayside ionopause streamlined by the stellar wind as a semi-sphere, which radius is determined by pressure balance between the planetary flow and stellar wind at the
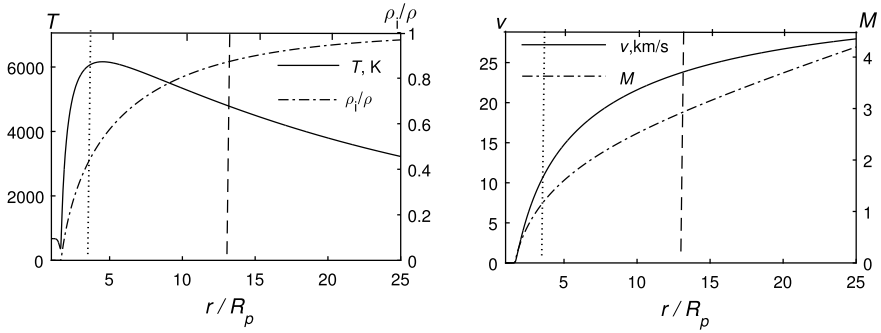
Fig. 3 Temperature and ion fraction (left panel), velocity and sonic Mach number (right panel) as functions of the radial distance for exoplanet TOI-421c. The dotted and dashed vertical lines mark the critical sonic point and the ionopause position, respectively

central stagnation point. The 1-D upper atmosphere model yields supersonic radial flow of the atmospheric particles. Using the calculated profiles of the atmospheric density, velocity, and pressure, we determine the distance from the planet to the stagnation point, where the atmospheric pressure is equal to the stellar wind total pressure P_{tot}^*. The latter is proportional to the dynamic pressure $P_{tot}^* = K\rho_{sw}v_{sw}^2$, where the subscript "sw" denotes the undisturbed stellar wind parameters. The coefficient K depends on the IMF considered in our stellar wind model. The ionopause is considered to be penetrable for the neutral atmospheric particles, but impenetrable for the ions. Therefore the neutral atmospheric atoms can cross the ionopause and penetrate the stellar wind region, where they are ionized and load the stellar wind flow. The calculation domain for the stellar wind flow is between the upper boundary upstream of the shock front and the ionopause approximated by the semi-sphere. At the upper boundary we set the undisturbed stellar wind parameters. At the ionopause we set the boundary conditions for normal components of the stellar wind velocity and magnetic field assumed to vanish. Also at this boundary we set density and radial velocity of the neutral hydrogen atoms obtained from the 1-D upper atmosphere model. In the region of stellar wind flow around the ionopause we solve the ideal MHD equations including the source terms related to interaction between stellar wind and the atmospheric neutral particles [14, 15]

$$\frac{\partial(\rho_i \mathbf{v})}{\partial t} + \nabla \cdot \left[\rho_i \mathbf{v}\mathbf{v} + \mathbf{I}\left(p + \frac{B^2}{8\pi}\right) - \frac{\mathbf{B}\mathbf{B}}{4\pi} \right] = S_i \mathbf{v_a} - S_{ex}(\mathbf{v} - \mathbf{v_a}), \quad (23)$$

$$\frac{\partial W}{\partial t} + \nabla \cdot \left[\frac{1}{2}\rho_i v^2 \mathbf{v} + \frac{\gamma}{\gamma - 1}p\mathbf{v} + \frac{1}{4\pi}\mathbf{B} \times (\mathbf{v} \times \mathbf{B}) \right] =$$
$$(S_i + S_{ex})\left(\frac{1}{2}v_a^2 + \frac{3kT_a}{2m}\right) - S_{ex}\left(\frac{1}{2}v^2 + \frac{3kT}{2m}\right), \quad (24)$$

$$W = \frac{1}{2}\rho_i v^2 + \frac{1}{\gamma - 1}p + \frac{1}{8\pi}B^2, \quad (25)$$

$$\frac{\partial \mathbf{B}}{\partial t} - \nabla \times (\mathbf{v} \times \mathbf{B}) = 0, \tag{26}$$

$$\frac{\partial \rho_i}{\partial t} + \nabla \cdot (\rho_i \mathbf{v}) = S_i, \tag{27}$$

$$\nabla \cdot \mathbf{B} = 0, \tag{28}$$

where ρ_i, $\mathbf{v}$, p, and $\mathbf{B}$ are the proton mass density, velocity, plasma pressure, and magnetic field in the stellar wind, respectively. The parameter γ is the polytropic index (assumed to be 5/3), while v_n and T_n are the velocity and temperature of the neutral atoms leaving the atmosphere and entering the stellar wind. The momentum, energy, and mass conservation Eqs. (23), (24), (27) include source terms due to mass loading with parameters S_i and S_{ex} corresponding to photo-ionization and charge exchange processes:

$$S_i = \nu \rho_n, \quad S_{ex} = \rho_i < V_{rel} > \rho_n \sigma_{ex}/m. \tag{29}$$

Here, ρ_n is the mass density of the neutral hydrogen atoms, σ_{ex} ($\sim 10^{-15} \, \text{cm}^2$) is the charge exchange cross section, $< V_{rel} >$ is the average relative speed of the stellar wind and atmospheric particles, and ν is the ionization rate defined above. We apply the numerical method based on the Godunov-type finite difference scheme in spherical coordinate system, which was described in [14].

The stellar wind stream is loaded with planetary ions, which arise as a result of photo-ionization and charge exchange processes. This leads to a strong deceleration of the stellar wind plasma and a corresponding increase in the magnetic field in front of the ionopause. In our model, the dayside ionopause is considered as a semi-sphere, similarly to [14]. The MHD calculation area is bounded by the streamlined surface and the outer semisphere, where the unperturbed stellar wind parameters are given. The normal components of the stellar wind velocity and interplanetary magnetic field are assumed to vanish at the ionopause.

6 Results of MHD Calculations

The stationary solution of the stellar flow problem around the ionopause was obtained by integrating non-stationary MHD equations over a sufficient long time. The stellar wind parameters used for calculations are as follows

$$v_{sw} = 240 \, \text{km/s}, \quad n_{sw} = 1500 \, \text{cm}^{-3}, \quad T_{sw} = 3.4 \cdot 10^5 \, \text{K},$$
$$B_{sw} = 3.54 \cdot 10^{-3} \, \text{G}, \quad M_s = 3.5, \quad M_A = 1.2. \tag{30}$$

The velocity v_{sw}, density n_{sw}, and temperature T_{sw} are taken from [13], and the magnetic field B_{sw} is determined by scaling the solar wind IMF at the Earth orbit (1 AU) to the orbital distance of the exoplanet TOI-421c (0.119 AU). Pressure balance at
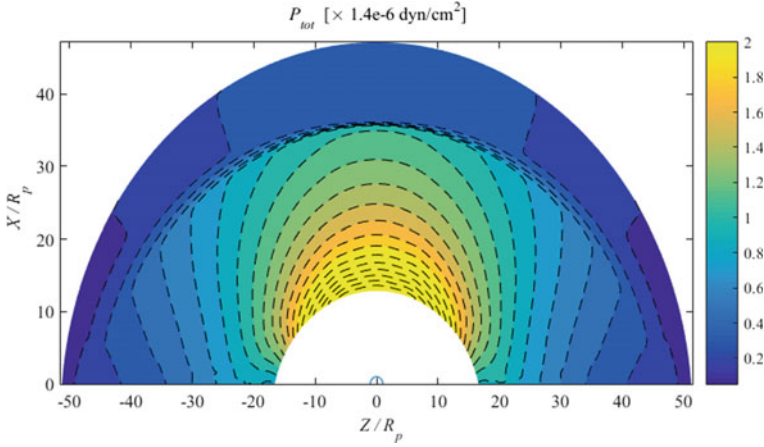
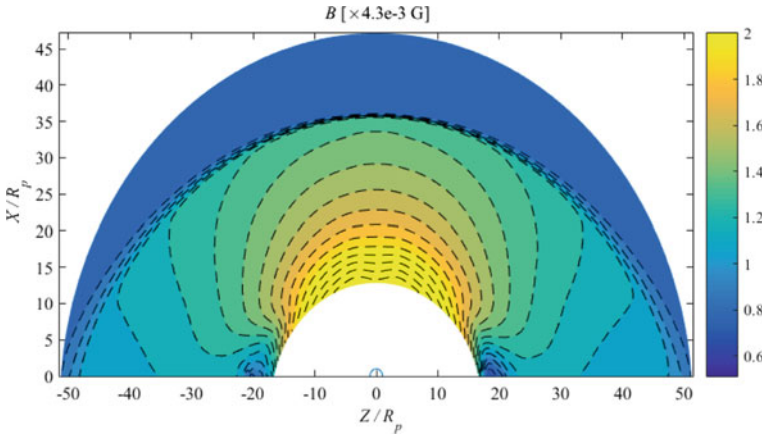**Fig. 4** Total pressure distribution in the magnetosheath

Fig. 5 Distribution of the total magnetic field strength

the stagnation point was established iteratively after several runs. The radial distance to the stagnation point was obtained about $13R_p$. Figure 4 shows the calculated distribution of the total pressure (the sum of the magnetic and plasma pressures) in the region of the stellar wind flow (plane XZ). The total pressure is enhanced substantially in the region of the disturbed stellar wind that is between the shock front and the obstacle boundary (ionopause). The maximum value is reached in the stagnation point. The distance between the shock front and the stagnation point is about $23R_p$. Figure 5 is similar to Fig. 4, but presents the distribution of the magnetic field strength in the flow region. The magnetic field sharply increases at the front of the shock wave, and then increases significantly when approaching the ionopause. We call the region of enhanced magnetic field as "magnetic barrier region". Figure 6
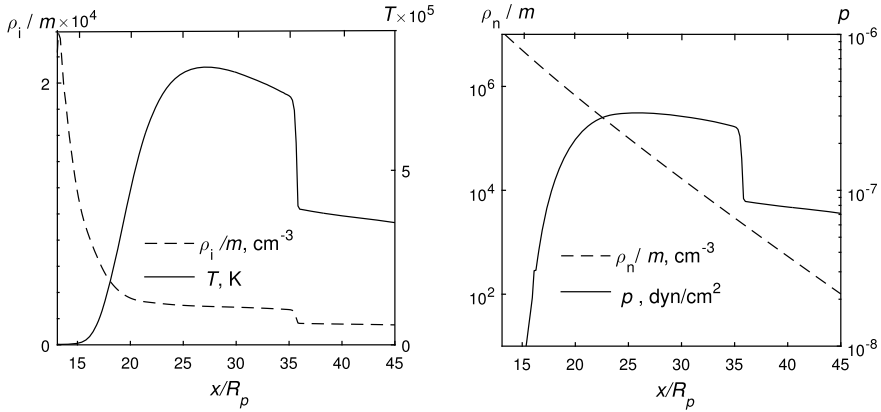
Fig. 6 Profiles of proton density and temperature (left panel), neutral atom density and thermal pressure (right panel) along the stagnation line

shows the proton density and temperature on the left side, hydrogen atom density and plasma pressure on the right side as functions of the radial distance along the stagnation line. The pressure and temperature decrease very strongly in the region of the magnetic barrier. At the same time, the proton density increases quite sharply towards stagnation point due to capture of the atmospheric ions produced by photo-ionization and charge exchange processes in the region of stellar wind flow around the ionopause. Figure 7 presents the profiles of the total pressure (left panel), magnetic field strength, and velocity (right panel) between the stagnation point and the shock front. The velocity drops sharply at the front of the shock wave, and then decreases monotonically towards the stagnation point. But the magnetic field intensity and total pressure show a sudden jump at the shock front, and a subsequent gradual increase towards the ionopause. This growth increases as we approach the streamlined surface. The total pressure maximum exceeds the stellar wind dynamic pressure in 2.7 times.
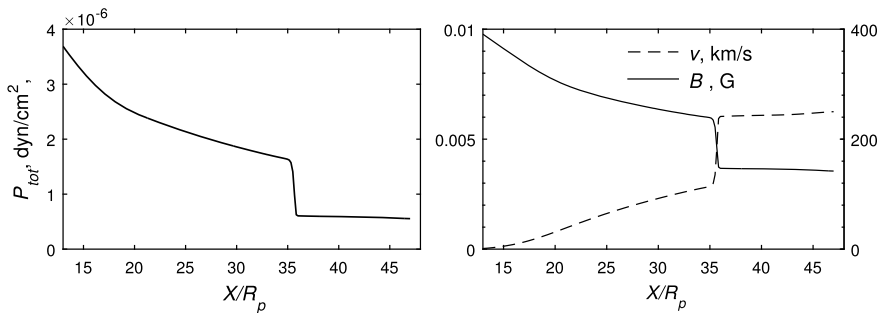

Fig. 7 Profiles of the total pressure (left panel), magnetic field strength and velocity (right panel) along the stagnation line
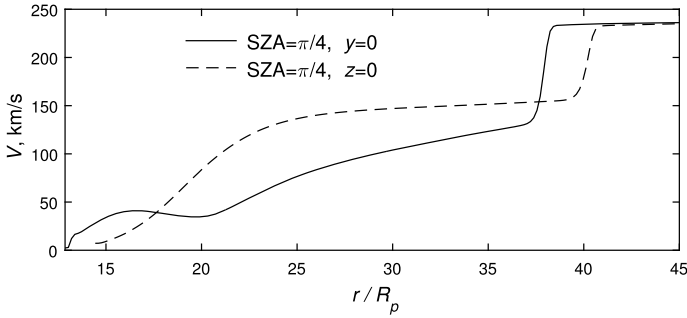
Fig. 8 Stellar wind velocity profiles along the radial directions in two planes ($Y = 0$ and $Z = 0$) for the fixed stellar-zenith angle (SZA), which is between the radial direction and X axis pointed to the host star

With this total pressure, the stagnation point is disposed at the distance $\sim 13R_p$ from the center of planet. In case of pure hydrodynamic stellar wind without IMF, the magnetic pressure vanishes and the external gas pressure at the stagnation point becomes slightly less than the stellar wind dynamic pressure. In this case, without IMF, the stellar wind stagnation point would be located at a distance of about $23R_p$, which is 1.8 times greater than in the case with the IMF.

Figure 8 shows stellar wind velocity as a function of the radial distance in two planes: $Y = 0$, and $Z = 0$. One plane ($Y = 0$) is coplanar to the IMF vector, and another plane ($Z = 0$) is orthogonal to the IMF vector. In a case without a magnetic field, the velocity profiles would be identical to each other in these two planes. But magnetic field brings a strong asymmetry between planes parallel and perpendicular to the IMF. Figure 9 shows the total pressure (left panel) and the magnetic field strength (right panel) as functions of the stellar-zenith angle (SZA) measured from the x axis for various radial distances. The solid curve 1 is located along the ionopause,
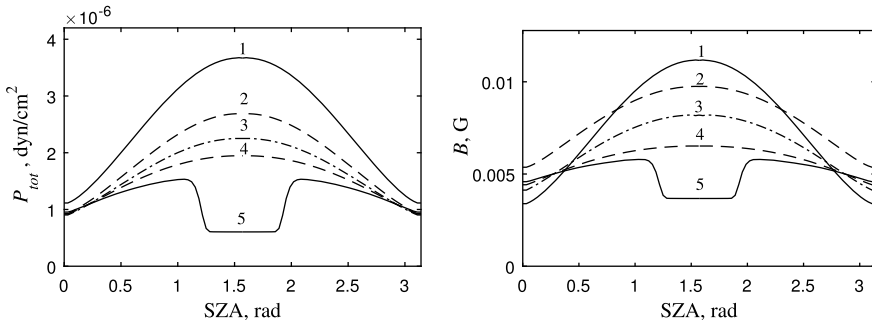

Fig. 9 The total pressure (left panel) and the magnetic field strength (right panel) as functions of the stellar-zenith angle (SZA) for different radial distances: curves 1, 2, 3, 4, 5 correspond to $r/R_p = 13, 18, 23, 28, 36$, respectively

and the solid curve 5 is along the trajectory in vicinity of the shock wave. The central part of this curve (where the magnetic field is weakened) corresponds to the region of the undisturbed stellar wind upstream of the shock wave.

7   Conclusion

Our study considers the recently discovered exoplanet TOI-421c. EUV heating of the upper atmosphere results in supersonic atmospheric wind interacting with the incoming magnetized stellar wind. In particular, we focus on effects related to the stellar wind magnetic field. The first important factor is that exoplanet TOI-421c is located much closer to the host star than the planets of the solar system: its orbital distance is 6 times less than that of Venus. Because of this, the IMF is much stronger compared to Venus, and the Alfvén Mach number only slightly exceeds 1. The second important factor is that an intense radial flow of atmospheric gas penetrates into the region of the stellar wind, where hydrogen atoms are ionized and mixed with the stellar wind plasma, causing its deceleration. The intense mass loading of the stellar wind plasma due to the ionization of atmospheric neutral particles leads to a substantial increase in magnetic field strength and the corresponding decrease in pressure, velocity, and temperature of the plasma. The obtained results of simulation highlight new important features of the magnetic barrier in front of the exoplanet. Compared to the purely hydrodynamic simulations without a magnetic field [13], we found that the presence of a magnetic field in the stellar wind radically changes the whole picture of interaction of the stellar wind with the atoms of the atmosphere. In particular, interplanetary magnetic field makes crucial influence on the radius of the ionopause, as well as on the profiles of the plasma density, pressure and temperature between the ionopause and the bow shock. The bow shock position is also strongly dependent on the IMF intensity. The stellar wind flow around the ionopause has a very strong asymmetry caused by the magnetic field. The plasma velocity along the magnetic field is much less than in the direction perpendicular to the magnetic field. The region of highly enhanced magnetic pressure (magnetic barrier) is much thicker for the exoplanet compared to Venus. In this case the magnetic pressure dominates over the gas pressure in the entire region of the MHD flow. Maximum magnetic and total pressure at the stagnation point is much higher than the dynamic pressure of the stellar wind. The enhanced magnetic field shifts the boundary of the atmosphere (ionopause) to a position that is much closer to the planet, compared with the case of neglecting the interplanetary magnetic field. Meanwhile, the magnetic field pushes the shock front outward from the planet.

References

1. Zhang T. L., Luhmann J. G., Russell C. T.: The magnetic barrier at Venus. J. Geophys. Res. 96, 11145–11153 (1991). https://doi.org/10.1029/91JA00088
2. Biernat, H. K., Erkaev, N. V., Farrugia, C. J.: Aspects of MHD flow about Venus. Journal of Geophysical Research. 104, A6, 12617–12626 (1999). https://doi.org/10.1029/1999JA900032
3. Erkaev, N. V., Bößwetter, A., Motschmann, U., Biernat, H. K.: Aspects of solar wind interaction with Mars: comparison of fluid and hybrid simulations. Annales Geophysicae. 25, 1, 145–159 (2007). https://doi.org/10.5194/angeo-25-145-2007
4. Erkaev, N. V., Farrugia, C. J., Biernat, H. K.: Effects on the Jovian magnetosheath arising from solar wind flow around nonaxisymmetric bodies. Journal of Geophysical Research. 101, A5, 10665–10672. https://doi.org/10.1029/95JA03518
5. Erkaev N., Mezentsev A., Biernat H.: Influence of the interplanetary magnetic field on the solar wind flow about planetary obstacles. Space Science Reviews. 122, 209–219 (2006). https://doi.org/10.1007/s11214-006-6059-z
6. Erkaev, N.V., Lammer, H., et al.: XUV exposed non-hydrostatic hydrogen-rich upper atmospheres of terrestrial planets. Part I: Atmospheric expansion and thermal escape. Astrobiology Journal. 13, 1011–1029 (2013). https://doi.org/10.1089/ast.2012.0957
7. Erkaev, N.V., Lammer, H.., et al.: EUV-driven mass-loss of protoplanetary cores with hydrogendominated atmospheres: the influences of ionization and orbital distance. Monthly Notices of the Royal Astronomical Society. 460, 1300–1309 (2016). https://doi.org/10.1093/mnras/stw935
8. Murray-Clay, R. A., Chiang, E. I., Murray, N.: Atmospheric escape from Hot Jupiters. Astrophysical Journal. 693, 23–42 (2009). https://doi.org/10.1088/0004-637X/693/1/23
9. R. Hixon, Evaluation of a high-accuracy MacCormack-type scheme using benchmark problems. J. Comput. Acoustics 6, 291–305 (1998). https://doi.org/10.1142/S0218396X9800020X
10. Hixon, R., Turkel, E..: Compact implicit MacCormack-type schemes with high accuracy. Journal of Computational Physics. 158, 51–70 (2000). https://doi.org/10.1006/jcph.1999.6406
11. Gorbunova, K.D., Erkaev, N.V.: Compact MacCormac-type schemes applied for atmospheric escape problem. Journal of Siberian Federal University. Mathematics & Physics. 15(4), 500–509 (2022). https://doi.org/10.17516/1997-1397-2022-15-4-500-509
12. Carleo, I., Gandolfi, D., Barragán, O., et al.: The multiplanet system TOI-421: A warm Neptune and a super puffy Mini-Neptune transiting a G9 V star in a visual binary. The Astronomical Journal. 160, 114 (2020). https://doi.org/10.3847/1538-3881/aba124.
13. Berezutsky, A. G., Shaikhislamov, I. F., Rumenskikh, S., Khodachenko, M. L., Lammer, H., Miroshnichenko, I. B.: On the transit spectroscopy features of warm Neptunes in the TOI-421 system, revealed with their 3D aeronomy simulations. Monthly Notices of the Royal Astronomical Society. 515, 706–715 (2022). https://doi.org/10.1093/mnras/stac1633
14. Erkaev, N. V., Odert, P., Lammer, H., Kislyakova, K. G., Fossati, L., Mezentsev, A., Johnstone, C. P., Kubyshkina, D., Shaikhislamov, I. F., Khodachenko, M. L.: Effect of stellar wind-induced magnetic fields on planetary obstacles of non-magnetized hot Jupiters. Monthly Notices of the Royal Astronomical Society. 470, 4330–4336 (2017). https://doi.org/10.1093/mnras/stx1471
15. Odert, P., Erkaev, N. V., Kislyakova, K. G., Lammer, H., Mezentsev, A. V., Ivanov, V. A., Fossati, L., Leitzinger, M., Kubyshkina, D., and Holmström, M.: Modeling the Lyα transit absorption of the hot Jupiter HD 189733b. Astronomy & Astrophysics. 638, A49 (2020). https://doi.org/10.1051/0004-6361/201834814